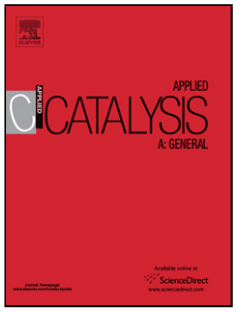

Isotopic study of the $La_{0.7}Ag_{0.3}MnO_{\delta\leq3}$ perovskite-catalyzed soot oxidation in presence of NO

Laura Urán (Conceptualization) (Validation) (Formal analysis) (Investigation) (Writing - original draft) (Visualization) (Data curation), Jaime Gallego (Formal analysis) (Funding acquisition), Esther Bailón-García (Writing - review and editing) (Validation) (Formal analysis), Agustín Bueno-López (Conceptualization) (Resources) (Methodology) (Validation) (Writing - review and editing) (Funding acquisition), Alexander Santamaría (Supervision) (Project administration) (Funding acquisition)

PII: S0926-860X(20)30204-0

DOI: https://doi.org/10.1016/j.apcata.2020.117611

Reference: APCATA 117611

To appear in: *Applied Catalysis A, General*

Received Date: 3 March 2020

Revised Date: 23 April 2020

Accepted Date: 28 April 2020

Please cite this article as: Urán L, Gallego J, Bailón-García E, Bueno-López A, Santamaría A, Isotopic study of the $La_{0.7}Ag_{0.3}MnO_{delta}$ perovskite-catalyzed soot oxidation in presence of NO, *Applied Catalysis A, General* (2020), doi: https://doi.org/10.1016/j.apcata.2020.117611

Isotopic study of the $La_{0.7}Ag_{0.3}MnO_{\delta\leq3}$ perovskite-catalyzed soot oxidation in presence of NO.

Laura Urán[a], Jaime Gallego[a], Esther Bailón-García[b], Agustín Bueno-López[b] and Alexander Santamaría[a,*]

[a] Química de Recursos Energéticos y Medio Ambiente, Instituto de Química, Facultad de Ciencias Exactas y Naturales, Universidad de Antioquia (UdeA), Calle 70 N_0 52-21, 1226 Medellín, Antioquia, Colombia

[b] Departamento de Química Inorgánica, Universidad de Alicante, Carretera de San Vicente s/n. E03080, Alicante, España

[*]Corresponding author.
E-mail address: alexander.santamaria@udea.edu.co (A. Santamaría)

Graphical abstract

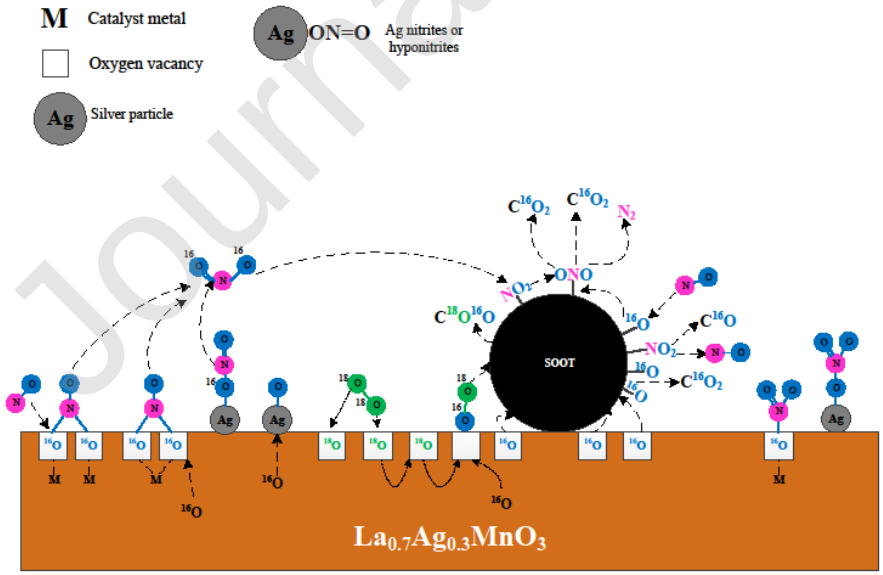

Highlights

- Ag-promoted oxygen exchange enhances soot and NO oxidation capacity
- Oxygen active sites, and silver particles enhance oxygen exchange capacity
- Weakly NO_x-adsorbed species lead to NO_2 desorption and soot-oxidation assistance
- Oxygens coming from catalyst starts soot oxidation process
- O_2 and NO compete for the same active sites

Abstract

Soot oxidation process over $La_{0.7}Ag_{0.3}MnO_{\delta\leq3}$ (LAM) and $LaMnO_3$ (LM) catalysts was studied through $^{18}O_2$ isotopic labelling experiments in the presence and absence of NO, using catalyst-soot mixtures under loose contact conditions. Isotopic exchange experiments evidenced that silver-particles enhanced oxygen exchange capacity, explained by the increase of oxygen active sites formed due to the charge compensation mechanism in the perovskite-like structure due to silver incorporation, and metallic-silver-segregated on catalytic surface. This enhanced oxygen exchange ability leads to the improvement of the catalytic soot oxidation capacity.

The elucidated reaction-pathway indicated that catalyst oxygen is transferred to soot, and then gas-phase-oxygen occupies the vacancies created. Furthermore, 16-oxygen species coming from catalyst play an important role in the formation of NO_x-adsorbed species that lead to NO_2 formation, which assists soot oxidation. The desorption of NO_2 was favored with Ag-particles presence because it promoted the formation of less thermally stable adsorbed NO_x species.

Keywords

$La_{0.7}Ag_{0.3}MnO_{\delta\leq3}$ perovskite-like catalyst; isotopic oxygen exchange; soot oxidation; NO_x; metallic silver sites

1. Introduction

The application of diesel engine is growing rapidly because of the high efficiency of the engines, and their low-operating costs. However, the diesel engine is one of the largest contributors to the emissions of diesel particulate matter (DPM) and NO_x [1–4]. DPM and NO_x emission regulation have become more and more stringent, e.g., Euro VI regulations started to control the number of particles emitted. Thus, effective emissions control devices need to be developed to enable vehicles to meet the increasingly stringent limits [4]. In this sense, the most widely used approach is to trap DPM in a porous ceramic wall flow diesel particulate filter (DPF) [4], which has high filtration efficiency of particles (>99 %) [5]. As the filter accumulates particle matter, engine backpressure increases and it is required a periodic regeneration of the filter by burning the trapped soot. However, soot oxidation temperature is above 600 °C, and the temperature of diesel exhaust gases, which is usually below 450 °C, is not enough to ignite soot [6]. Then, the use of filters with catalyst coated on their porous walls become an alternative to decrease soot oxidation temperature up to the range of diesel exhaust gases temperature, and to continuously regenerate the filter after soot deposition. DPF based on noble-metal-catalysts are the ones commercially available [7–9], being noble metals very active, but very expensive [10]. Therefore, alternative materials like mixed oxides have become studied as catalysts for DPF [11–21]. Among the studied alternatives, perovskite-like materials are very attractive due to their high activity, mostly related with their ability to produce active oxygen species [22]. Perovskite-like materials have the versatility to adopt a wide range of different compositions, with the change of either the A or the B cation, or the partial substitution of each cation by other cations, either with the same or different valences. These changes allow the formation of oxygen vacancies, or changes in the chemical state of A- and/or B-site elements; or segregation of metal particles on catalyst surface; all these surface defects turn into an improvement of catalytic activity [23–25].

Wang et al (2010) [26] studied the effect of partial substitution of La^{3+} cation with silver Ag^{+} in $LaMnO_3$ perovskite lattice on catalytic activity for soot oxidation in presence of NO. According to this study, the $La_{0.7}Ag_{0.3}MnO_3$ catalyst reduced the soot combustion temperature in about 40 °C and increased the NO conversion towards N_2 in almost 10% compared to $LaMnO_3$. The authors indicated that the partial substitution of Ag^{+} at A-site ions enhanced catalytic activity due to the increase of oxygen vacancy concentration and the over-stoichiometric oxygen content. The oxygen vacancy is beneficial because it enhances the adsorption and activation of NO or molecular oxygen. Additionally, the existence of metallic Ag in catalyst surface speeds up the combustion rate of soot, and promotes the reduction rate of NO toward N_2.

In our previous study, we addressed the effect of synthesis methodology of $La_{0.7}Ag_{0.3}MnO_{\delta\leq3}$ solid on catalytic soot oxidation in presence of NO. We have found that the solid synthetized by microwave-assisted methodology (MW) had a better silver incorporation into perovskite lattice resulting in a higher oxygen vacancies content. In addition, there was found a synergistic effect between oxygen vacancies and metallic silver particles on catalytic surface that enhances both soot oxidation activity (T_{50} = 371 °C, 100% CO_2 selectivity) and NO conversion (aprox. 64% by wt) mostly toward N_2. [27]. In another work, Yoon et al. [28], found that the partial substitution of La^{3+} with Ag^{+} in $LaMnO_3$ perovskite catalyst produced oxygen vacancies as active reaction sites for NO adsorption involving the formation of both mono- and bi-dentate nitrate species as the major reaction intermediates during the oxidation of NO to NO_2.

Considering that silver presence in $LaMnO_3$ perovskite lattice has an important role in the formation of oxygen sites, and/or active oxygen species for soot oxidation and NO adsorption, the study of the role of catalyst oxygen in soot combustion mechanism is necessary for improvement of these promising materials. Isotopic experiments have been useful to study catalyst-oxygen-exchange capability, as a measurement of active oxygen species formation, since labeled gases experiment allows the study of reaction pathways [6,22]. Serve et al. [22] investigated the potential synergy between Ag nanoparticles and Yttria-Stabilized Zirconia (YSZ), for soot oxidation in the developing of an efficient and stable catalyst for Diesel Particulate Filter regeneration with molecular oxygen. From isotopic oxygen experiments, the authors prove the participation of active oxygen species originated from the YSZ lattice. Furthermore, it was stablished that silver promoted soot oxidation activity by activating the dissociative adsorption and lattice integration of gaseous oxygen.

Guillén-Hurtado et al. [14] studied the ceria-catalyzed soot oxidation by a pulse technique with labeled O_2 in the presence of NO. The authors stablished that, in the absence of soot, the ceria-catalyzed oxidation of NO to NO_2 takes place with ceria oxygen and not with gas-phase O_2. They also said that gas-phase O_2 did not react directly with soot, when O_2-pulsed experiments were carried out over a soot-ceria loose contact mixture. Instead, ceria oxygen is transferred to soot, and gas-phase O_2 fills up the vacancies created on the oxide surface in a further step. Furthermore, the authors found that in the presence of NO, NO_2 is expected to be additionally generated by ceria oxygen oxidation, which also reacts with soot.

Considering the promising behavior of Ag-doped $LaMaO_3$ perovskite and the potential of isotopic gases in the study of catalyst oxygen role in soot combustion, the main objective of this study is to

address the NO-assisted soot oxidation process over $La_{0.7}Ag_{0.3}MnO_{\delta\leq3}$ and $LaMnO_3$ catalysts, through $^{18}O_2$ isotopic labelling experiments.

2. Methodology

2.1 Sample preparation

$La_{0.7}Ag_{0.3}MnO_{\delta\leq3}$ (referred to as LAM) and $LaMnO_3$ (named LM) perovskite-like catalysts were synthesized by microwave-assisted (MW) methodology [27]. Reagent-grade metal nitrates: $La(NO_3)_3$ $6H_2O$ (Merck), $AgNO_3$ (Merck) and $Mn(NO_3)_2$ $4H_2O$ (Merck) were dissolved in deionized water. The solution was irradiated with ultrasonic irradiation for 30 min, and then stirred during 6 h. Subsequently, the resulting solution was subjected to microwave irradiation for 6 min at 700 W. Afterward, the solid sample was calcined in air at 600 °C for 1 h.

2.2 Catalyst characterization

Structural information of catalysts was examined by X-ray diffraction, using a Panalytical X'PERT PRO MPD diffractometer with Cu K_α radiation (λ = 1.5406 Å), operated at 45 kV and 40 mA. Measurement were carried out in a continuous scan mode from 10° to 70° (2θ) with a scan step size of 0.013° and step time of 1 minute.

Raman spectrum in the range of 100 cm^{-1} to 1000 cm^{-1} was recorded using a LabRam HR Horiba microscope system with a 632.8 nm He/Ne laser excitation source, a laser power of 0.17 mW, an exposure time of 1 s, and acquisition time of 10 s.

X-ray photoelectron spectroscopy (XPS), using a Thermo Fisher Scientific system equipped with an Al Kα X-ray source at an operating voltage of 20 kV and a current of 20 mA. All the binding energies were calibrated with the C1s binding energy fixed at 284.6 eV as an internal reference.

To establish nitrogen-adsorbed species on LAM and LM catalysts, In situ diffuse reflectance Fourier Transform (DRIFT) spectra were recorded on a Nicolet 6700 FTIR spectrometer, at a resolution of of 4 cm^{-1} in the wavenumber range from 1000 cm^{-1} to 4000 cm^{-1}. The IR cell was charged with soot–catalyst mixtures (1:9 weight ratio) that were prepared in tight contact and diluted with KBr. The sample inside the IR cell was pretreated in Ar stream (50 ml/min) at 500°C for 20 min to remove

surface adsorbed H_2O and CO_2. Afterward, the sample was exposed to a gas mixture of 2000 ppm NO/10% O_2/ Ar at a flow rate of 50 mL/min, and heating at a rate of 5 °C/min.

2.3 Catalytic performance test

Catalytic experiments were carried out in a tubular quartz reactor coupled to Specific NDIR-UV gas analyzers for CO, CO_2, NO, NO_2 and O_2 monitoring. The reactor was heated from room temperature to 700 °C at 5°C/min, and charged with a mixture of 25 mg of soot plus 225 mg of catalyst (1:9 weight ratio) and 750 mg of SiC, the sample was mixed with spatula (loose contact) during 10 min. The model soot used in this study consisted of a carbon black, FW200, from Orion Engineering. Different gas mixtures were used with 0 to 2000 ppm NO + 10% O_2 in N_2, and the gas flow was fixed at 500 ml/ min (GHSV=30,000 h^{-1}). Even though catalytic experiments were performed up to 700 °C, the calcination temperature was chosen at 600 °C; since some structural changes in perovskite phase were evidenced at higher calcination temperatures that we wanted to avoid (see Fig. S1 and Table. S1).

2.4 $^{18}O_2$ isotopic-labelling experiments

Isotopic exchange experiments were carried out with $^{18}O_2$. The experimental set-up consisted of a several mass flow controllers, an injection valve with 100 µl loop, and two high sensitivity pressure transducers, which allow gas injections without pressure variation in the system. The gas composition was monitored with a mass spectrometer Pfeiffer Vacuum (model OmniStar). The experiments were carried out in a 5 mm inner diameter cylindrical fixed-bed reactor with 50 mg of catalyst plus 5.5 mg of soot mixed in the so-called loose contact mode. All samples were diluted with 166 mg of SiC and packed between plugs of quartz wool.

Prior to $^{18}O_2$ pulses, the sample (catalyst (cat), or catalyst-soot mixture (cat-soot)) was submitted to an in-situ pretreatment at 500 °C for 30 minutes under He atmosphere at a flow rate of 20 ml/min to remove surface-adsorbed (H_2O and CO_2) contaminants from catalysts (see Fig. S2). However, as it is hard to remove all surface carbonates during pretreatment, to make sure that remaining carbonates do not pollute CO_2 interpretation during soot oxidation experiments, or interfere in oxygen exchange interpretation as previously evidenced [22], we verified $C^{16}O_2$, $C^{18}O_2$ and $C^{16}O^{18}O$ mass spectroscopy signals during $^{18}O_2$ pulses over the catalysts alone (see Fig. S3 and Fig. S4).

After pretreatment, for pulse experiments, the reactor was cooled down to the desired temperature (200 °C, 300 °C or 400 °C). Then, the selected atmosphere, He (for cat, and cat-soot tests) or 800 ppm NO/He (for cat-NO, and cat-soot-NO tests), flowed inside the reactor all the time. However, in any case, the first pulse introduced into the gas stream corresponds to 100 µl of Ar to obtain the reference profile, since Ar does not chemically react with the catalyst or sample. Then, the following pulses consist of 100 µl of $^{18}O_2$, a species that reacts with the catalyst. Finally, by comparing the Ar (reference) and O_2 responses we can assess the extent of oxygen-sample interaction. Sample was changed between pulses at different temperatures to ensure that sample surface was always free of ^{18}O-oxygens before each pulse.

3 Results.

3.1. Catalyst characterization

Fig. 1 (A) y (B) show the X-ray diffraction pattern for LAM and LM catalysts. The strong reflexion at 32° along with other less intense diffraction lines coincide with the reference diffraction pattern confirming the perovskite-like phase formation. These results suggest that the addition of silver did not modify the parent structure. However, the XRD patterns reveals that peaks are shifted toward higher angles with silver dopping, as demonstrated in Fig. 1 (B). This is consistent with lattice contraction due to the substitution of La^{3+} ions (ionic radius 1.36 Å) with smaller Ag^{+} ions (1.28 Å). Additionally, the 2θ signals at 38.3°, 44.5°and 64.6° in Fig. 1 A, corresponding to metallic silver (Ag°), indicate that not all silver was incorporated into the perovskite structure. Secondary phases associated with non-incorporated silver reacting with Mn, as $Ag_{1.8}Mn_8O_{16}$ [29], were not evidenced in the present study. Fig. 2 corresponding to Raman scattering measurement indicates perovskite-like phase formation. The Raman spectra presenting two high frequency modes, Ag (~ 496 cm^{-1}) and B_1g (~620 cm^{-1}), typical of manganites [30], and are associated to Jahn Teller (JT) distortions of the corner-shared oxygen octahedra in $LaMnO_3$. The intensities ratio of the JT distortion (IAg/IBg) have been calculated for LM and LAM, and the results are presented in Table 1. The ratio decreases in the Ag-doped catalyst, which can be associated to an increase in both Mn^{4+} cations formation (or a decrease in Mn^{3+} cations) due to a charge compensation mechanism caused by the presence of a cation of lower valence, as Ag^{+} in the A site cation position of the ABO_3 perovskite-like structure [30].

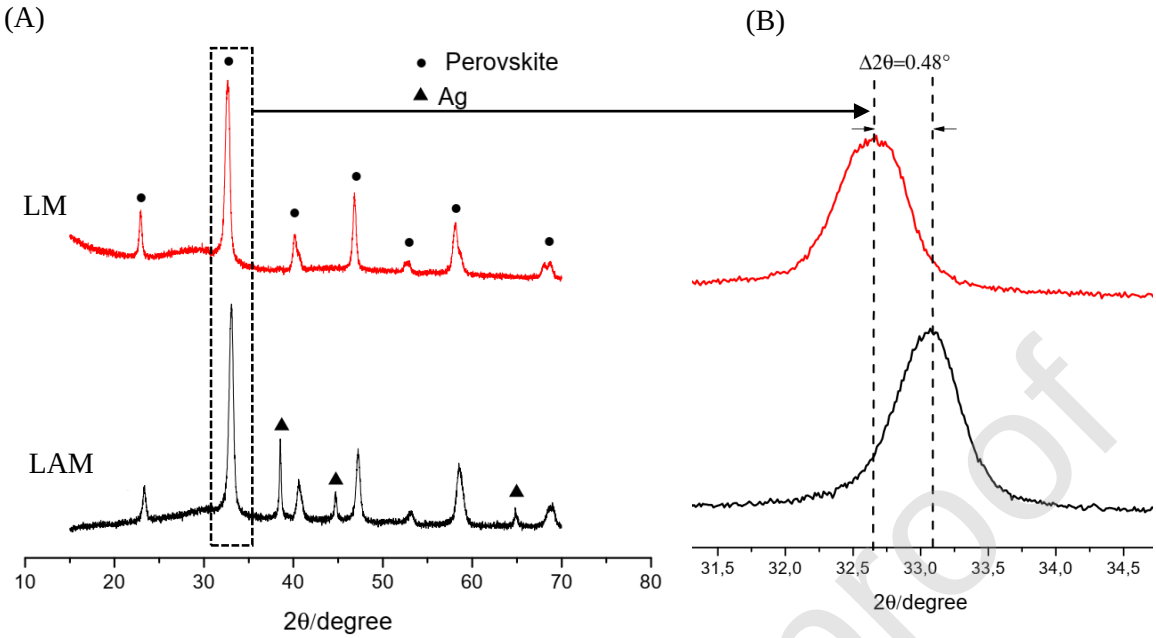

Fig. 1 (A) X-ray diffractogram of $La_{0.7}Ag_{0.3}MnO_3$ and $LaMnO_3$ catalysts. (B) shift of diffraction line at 32° toward higher 2θ.

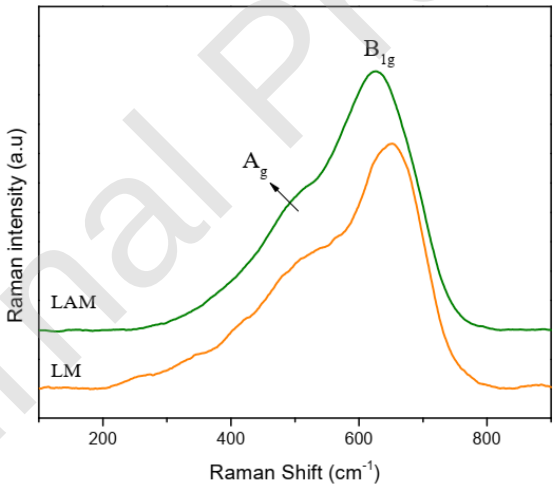

Fig. 2. Raman spectrum of LAM and LM catalysts.

X-ray photoelectron spectroscopy (XPS) analysis provides surface elemental composition and oxidation states of each element. Binding energies of La $3d_{5/2}$, Ag $3d_{5/2}$, Mn $2p_{3/2}$ and O 1s core levels were recorded by XPS for $LaMnO_3$ and $La_{0.7}Ag_{0.3}MnO_3$ perovskite-like samples (see Fig. 3).

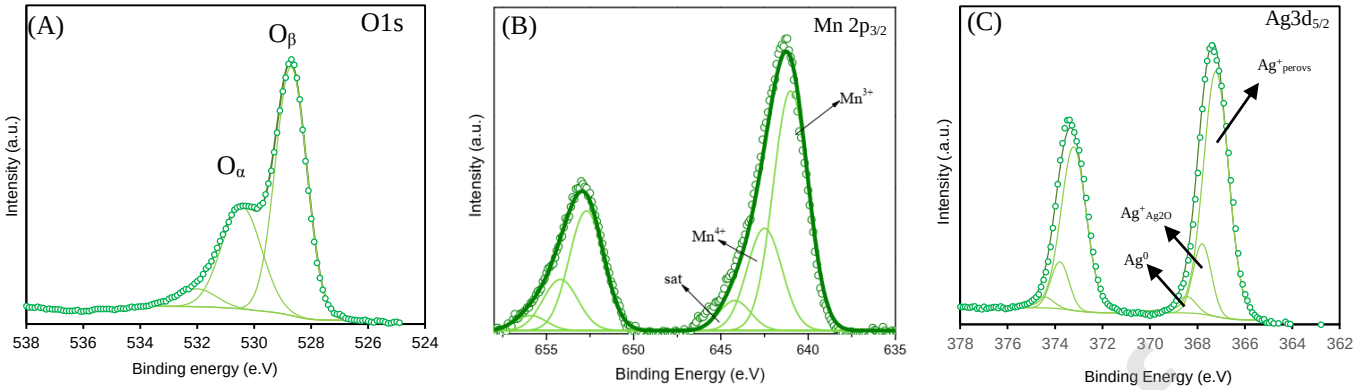

Fig. 3. Decomposed XPS spectra in the (A) O1s core level, (B) $Mn2p_{3/2}$ core level, and (C) $Ag3d_{5/2}$ of LAM perovskite-like catalyst.

From the XPS data, the O1s spectra were deconvoluted into three peaks around 528.6, 531, and 533.0 eV. The lower binding energy signal corresponds to lattice oxygen (O_β). Intermediate binding energy contribution is ascribed to adsorbed oxygen (O_α) on surface vacancies as O^- or O^{2-} species. The signal at the highest binding energy value is due to water and hydroxyl groups on the surface [31,32].

The $Mn2p_{3/2}$ spectra present three signals, corresponding to Mn^{3+} (641.3 eV) and Mn^{4+} (642.3 eV) and a weak satellite (644.0 eV) of the $Mn2p_{3/2}$ [31,33,34]. The $Ag3d_{5/2}$ spectra have three contributions associated to metallic silver (Ag^o) at 368.4 eV, segregated silver oxide (Ag_2O) at 367.8 eV and silver incorporated into perovskite lattice (Ag^+) at 367.2 eV [35]. In Table 1, the Ag/Mn atomic ratio higher than the stoichiometric one indicates that part of the silver was segregated on catalyst surface. Additionally, the charge compensation mechanism due to Ag^+ incorporation into perovskite-like lattice can be either by oxygen vacancies formation, as the increase in surface oxygen content (O_α) in LAM catalyst indicates; and/or by the shifting of B cation toward higher valences (e.g., Mn^{3+} to Mn^{4+}) [30], as the increase in the Mn^{4+}/Mn^{3+} atomic ratio states. These XPS results are in good agreement with the Raman results. Table 1 also shows BET surface area of LAM and LM catalysts, specific surface area values are relative low for both samples as expected for this kind of mixed oxides with negligible porosity [36–38]. However, it is evident that silver incorporation leads an increase in specific surface area, which in turns favored the exposure of LAM catalyst active sites as indicated for XPS results.

3.2 Catalytic performance

Fig. 4 shows the results of catalytic soot oxidation experiments under 10% O_2/N_2 and (10% O_2+1000 ppm NO)/N_2 flows over both $La_{0.7}Ag_{0.3}MnO_3$ (LAM) and $LaMnO_3$ (LM) catalysts (Fig. 4 A), and LAM/LM -catalyzed oxidation of NO to NO_2 in the absence of soot (Fig. 4 B). From Fig. 4 A, it is observed that LAM catalyst was more active toward soot oxidation in the absence of NO with a temperature for 50% of soot conversion (T_{50}) 10 °C lower than the one obtained for LM catalyst. Soot oxidation temperature decreased when NO was included in the gas flow of both catalytic systems, which was attributed to NO to NO_2 oxidation process. LAM solid was more active than LM material in the oxidation of soot, as well as in the oxidation of NO to NO_2. According to the profiles in Fig. 4 B, even though oxidation of NO started at 200 °C for both catalysts, the thermodynamic equilibrium was first achieved for LAM solid, around 370 °C, while LM solid achieved it at 427 °C. Selectivity toward CO_2 was always over 90% in both catalysts for all the performed tests (see Table 2). Even though the experimental results presented in this study are based on the loose contact between soot and catalyst, because it simulates diesel exhaust conditions[39], the influence on the type of contact was evaluated. Then, comparison between tight and loose contact is presented in Fig. S7.

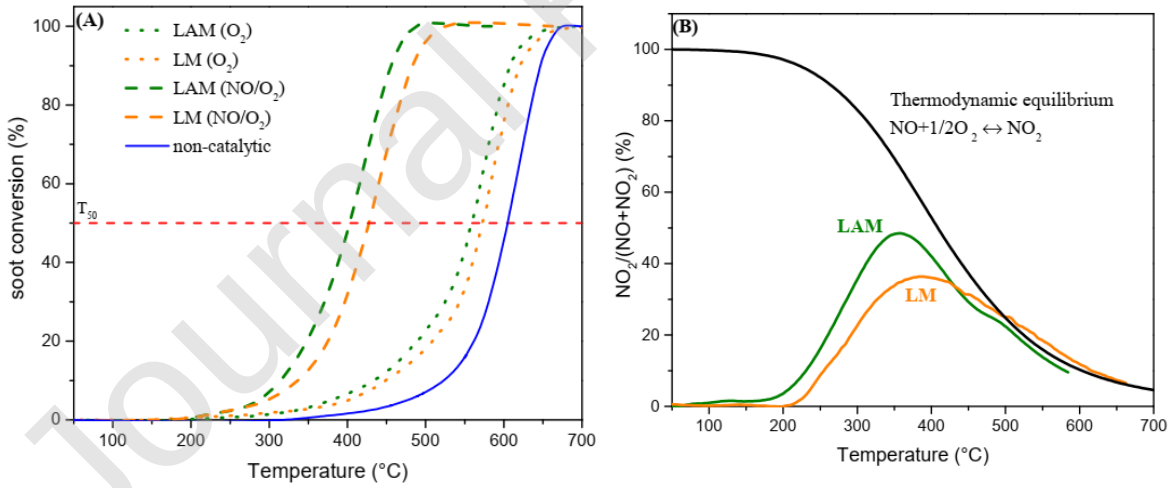

Fig. 4. (A) LAM and LM- catalyzed soot oxidation experiments under 10% O_2/N_2 and (1000 ppm NO + 10% O_2)/N_2 flows; and non-catalytic soot oxidation. (B) LAM and LM-catalyzed NO oxidation to NO_2 in the absence of soot (1000 ppm NO + 10% O_2) flow.

3.3 $^{18}O_2$ labeling experiments

This section presents $^{18}O_2$ labeling experiments results, which were divided in two parts. In the first one, the isotopic oxygen exchange capacity was evaluated for $La_{0.7}Ag_{0.3}MnO_3$ (LAM) and $LaMnO_3$ (LM) catalysts under different experimental conditions, while the second one presents the evolution profiles of the different species during soot oxidation with NO and $^{18}O_2$ pulsed.

A. Oxygen exchange under different conditions

To evaluate oxygen exchange over $La_{0.7}Ag_{0.3}MnO_3$ (LAM) and $LaMnO_3$ (LM) catalysts, $^{18}O_2$ was pulsed under different reaction conditions: only catalyst (cat), catalyst in presence of NO (cat-NO), catalyst soot mixture (cat-soot), and catalyst soot mixture in presence of NO (cat-soot-NO). Fig. 5 presents the profiles of the different oxygen species that leaved out the reactor after $^{18}O_2$ pulses over catalysts at 400 °C. This Figure showed that, for LAM, 64% of the O_2 molecules contain catalyst oxygen ^{16}O ($^{16}O_2$ and ^{16}O-^{18}O), 18% was not exchange ($^{18}O_2$), and the remaining 18 % was chemisorbed on the catalyst. For LM catalyst, only 23 % of the total $^{18}O_2$ pulsed was exchanged, and these results evidenced that LAM catalyst has higher oxygen exchange capacity. The above calculations are based on the comparison of the mass spectrometry signal responses of the different oxygen species at the reactor outlet, and the signal of Ar, which was used as reference and represents the 100 % of a pulse of 100 µl volume (see equations S1 and S2; tables S2 and S3). The higher oxygen adsorption capacity of LM catalyst is related with its higher basic character compared to LAM catalyst. Silver incorporation decreases the difference in electronegativity of the La-O bond (see Table S4), the one with the most basic character inside catalyst, decreasing its capacity to retain oxygen atoms. On the contrary, silver incorporation favored the oxygen exchange process as evidenced in the above.

It was also observed that the shape of oxygen species and Ar profiles were similar in both catalysts, indicating that the oxygen exchange occurs very fast. According to the XPS results (Table 1), the enhancement in oxygen mobility for LAM catalyst was possible due to the active sites formation created by both silver incorporation into perovskite lattice, and silver segregation on catalyst surface. Those active sites correspond to oxygen vacancies, reducible sites (Mn^{4+}) and metallic silver segregated on catalyst surface. According to Duprez et al (1996) [40], the release of $^{16}O_2$ is related to the presence of binuclear species such as O_2 , O_2^- or O_2^{2-} on catalyst surface, which are the active species that assure catalyst activity, widely named as α-oxygens [31,32,41]. This agrees with the

catalytic results, which evidenced a higher soot oxidation capacity of LAM catalyst under loose contact conditions (Fig. 4). Regarding the isotopic exchange mechanism, the presence of $^{16}O_2$ and $^{16}O^{18}O$ indicate that a multiple exchange mechanism occurs, where one molecule of labeled oxygen coming from gas phase ($^{18}O_2$) may exchange either one or both oxygen atoms with catalyst oxygen through a dissociative adsorption that follows equation 1 and 2 [40,42]

$$^{18}O^{18}O_{(gas)} + {}^{16}O_{(sup)} \rightleftharpoons {}^{18}O^{16}O_{(gas)} + {}^{18}O_{(sup)}$$
$$^{18}O^{16}O_{(gas)} + {}^{16}O_{(sup)} \rightleftharpoons {}^{16}O^{16}O_{(gas)} + {}^{18}O_{(sup)} \quad (1)$$

$$^{18}O^{18}O_{(gas)} + 2{}^{16}O_{(sup)} \rightleftharpoons {}^{16}O_{2(gas)} + 2{}^{18}O_{(sup)}$$
$$^{18}O^{16}O_{(gas)} + 2{}^{16}O_{(sup)} \rightleftharpoons {}^{16}O_{2(gas)} + {}^{16}O_{(sup)} + {}^{18}O_{(sup)} \quad (2)$$
$$^{18}O^{16}O_{(gas)} + 2{}^{18}O_{(sup)} \rightleftharpoons {}^{18}O_{2(gas)} + {}^{16}O_{(sup)} + {}^{18}O_{(sup)}$$

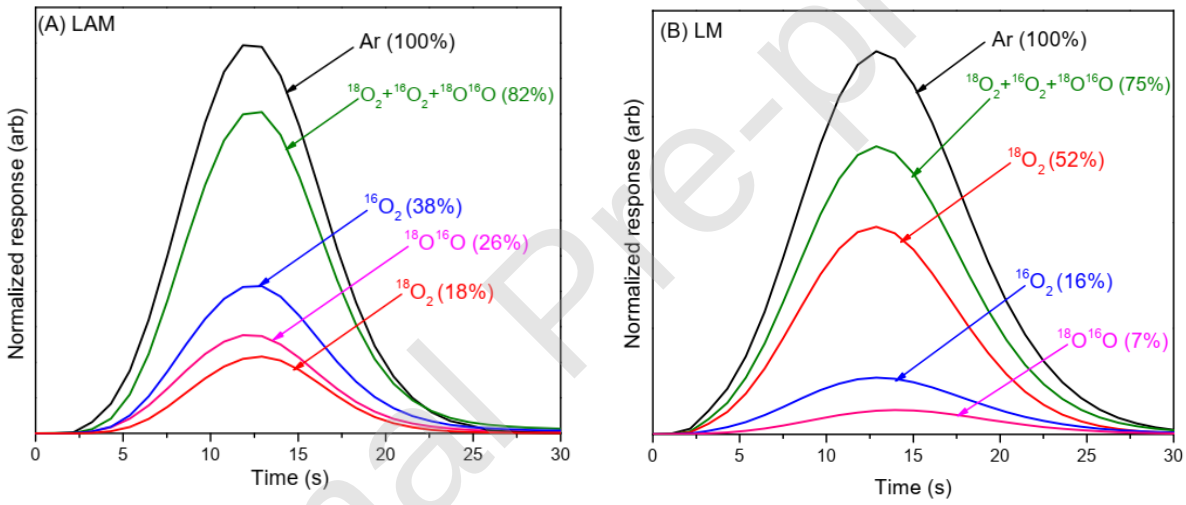

Fig. 5. Pulses of Ar and $^{18}O^{18}O$ at 400 °C over (A) $La_{0.7}Ag_{0.3}MnO_3$ (LAM) and (B) $LaMnO_3$ (LM).

Fig. 6 shows the contribution of the different isotopic oxygen species ($^{18}O_2$, $^{16}O_2$,$^{16}O^{18}O$) as a function of temperature for the different catalytic systems (open symbols: LAM; closed symbols: LM). Fig.6A shows that the oxygen exchange capacity for both catalysts in the absent of soot increases with temperature, being more evident for LAM catalyst. It is possible to see that over 300 °C the exchange of gas oxygens ($^{18}O_2$) with LAM catalyst oxygens is very fast due to the evolution of non-labelled oxygen (^{16}O-^{16}O) and scrambled oxygen (^{16}O-^{18}O) coming from catalyst. However, in presence of soot (Fig. 6 B) the quantity of oxygen-exchanged species ($^{16}O_2$,$^{16}O^{18}O$) significantly decreased even for LAM catalyst. This result can be explained by rapid consumption of the exchanged-oxygen species and $^{18}O_2$ pulsed during the soot oxidation process.

On the other hand, the presence of NO during the exchange experiments showed that, in the absence of soot (Fig. 6 C), the exchange of oxygen decreased at all the evaluated temperatures, compared with the exchange in the absence of NO (Fig. 6A). This result suggests that there is a competition between NO and O_2 for the same active sites over catalysts (LAM, LM), leading to the formation of nitrogen-containing species that latter will desorb as NO_2, as it is shown below (DRIFT results). This could be because NO reacts with oxygen coming from catalyst surface ($^{16}O_{sup}$) producing NO_2 (Fig. 7 E and F), which is more reactive. The inhibiting effect of NO on the oxygen exchange affects more to LAM than to LM, as deduced from Fig. 6D. Oxygen consumption, defined as the difference between the total oxygen pulsed and the sum of oxygen species measured after the exchange, became more significant over LAM catalyst due to its higher exchange capacity even at lower temperature (200°C) compared to LM. In fact, at 400 °C and in the presence of NO, the LAM catalyst consumed 40% of labelled oxygen compared to the 18% consumption over LM catalyst.

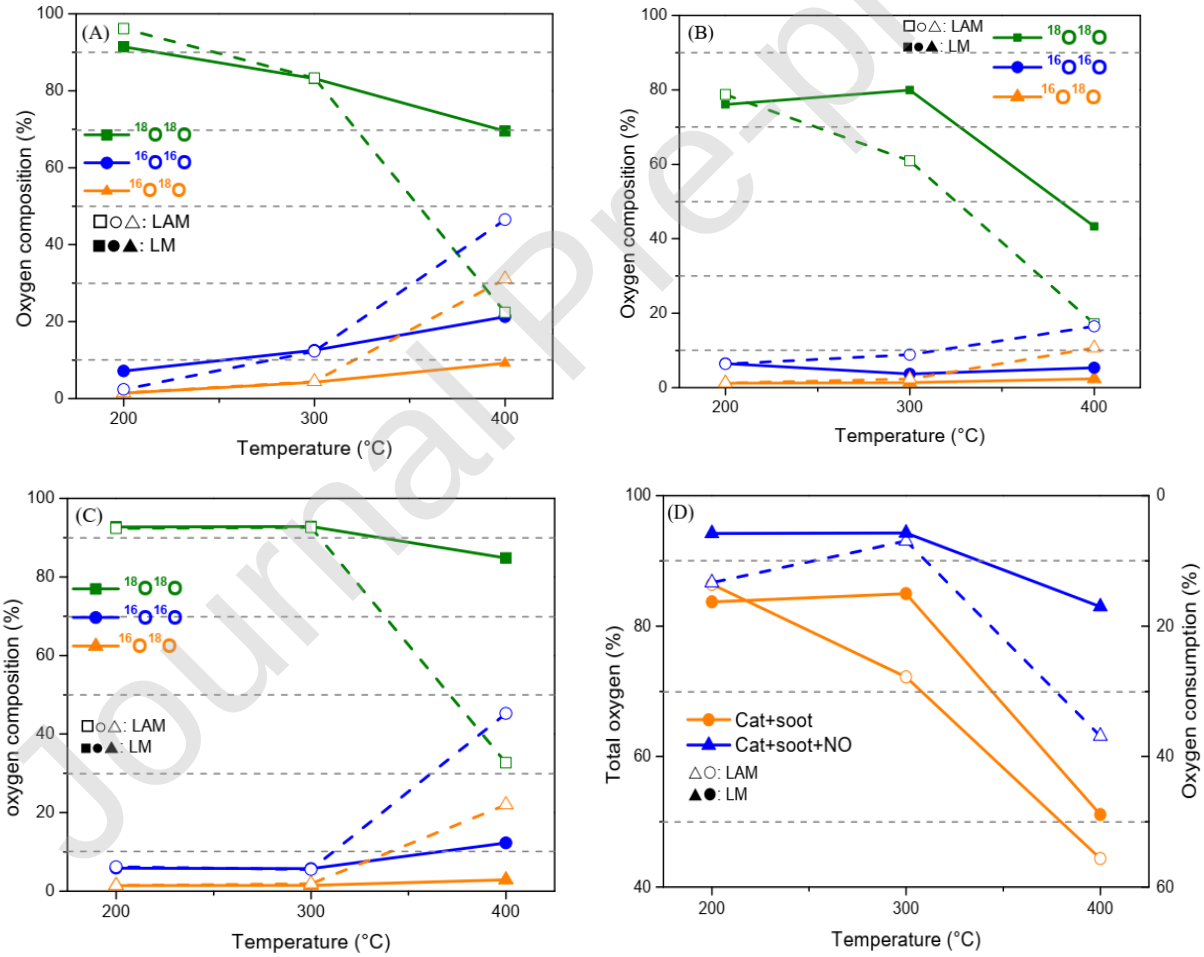

Fig. 6. Distribution of the different isotopic oxygen species ($^{18}O_2$, $^{16}O_2$,$^{16}O^{18}O$) as a function of temperature upon $^{18}O_2$ pulses evaluated at different conditions: only cat (A), cat-soot (B), and cat-

NO (C). Total oxygen consumption during cat-soot experiments under O_2 and O_2/NO atmospheres (D).

B. Evolution of the different species during soot oxidation process in presence of NO and labelled oxygen ($^{18}O_2$).

Fig. 7 shows the evolution of the different combustion species during soot oxidation process in the presence of NO and $^{18}O_2$ pulsed over LAM and LM catalysts at 400 °C.

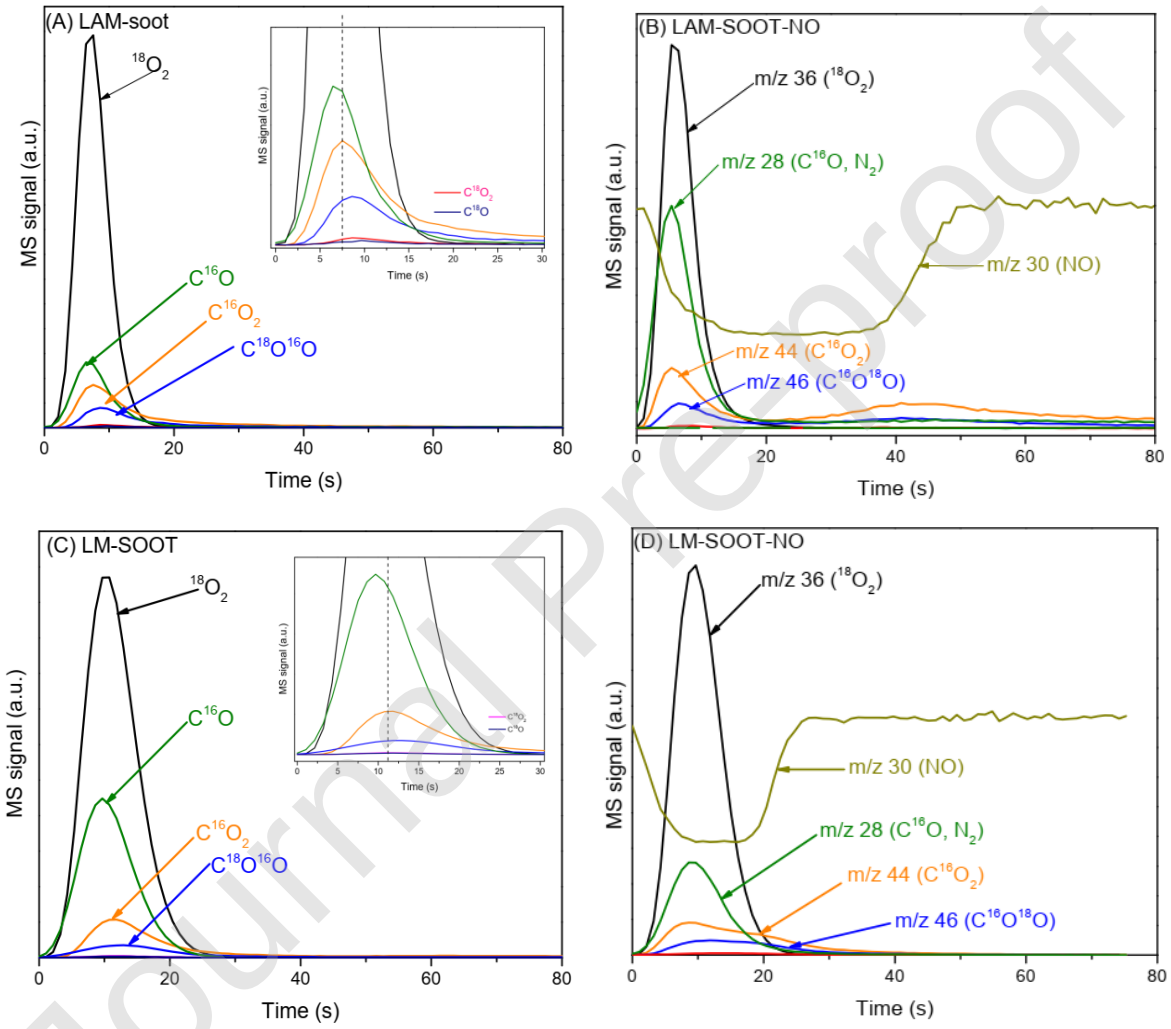

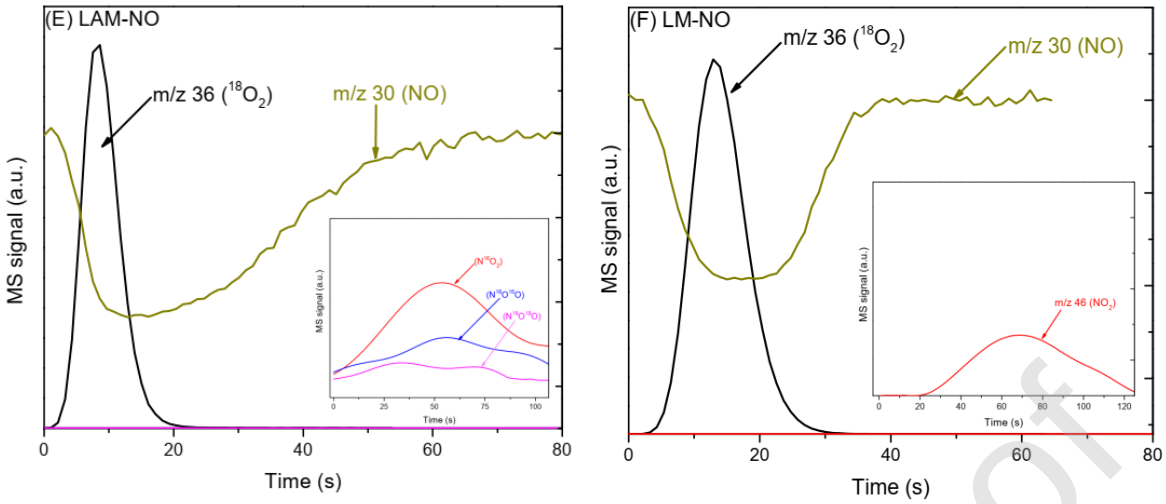

Fig. 7 Species evolution after $^{18}O_2$ pulses over LAM-soot (A), LAM-soot-NO (B), LAM-NO (E) and LM-soot (C), LM-soot-NO (D), LM-NO (F) samples.

In Fig. 7 A ($^{18}O_2$ pulses over LAM-soot), the $C^{16}O$ and $C^{16}O_2$ were the primary soot oxidation products suggesting that the oxygen from the catalyst ^{16}O was more reactive than oxygen from gas phase. Something similar was observed by Bueno et al. for a La-doped ceria catalyst, who stated that part of the labelled oxygen sticks to the catalyst activating the oxygen lattice which reacts with soot to produce CO and CO_2 with non-labelled oxygen [43]. The solid-solid reaction between catalyst and soot can be described with the step 1. The higher relative intensity of $C^{16}O$ signal compared to $C^{16}O_2$ must be attributed to the experimental conditions, since soot combustion is carried out in a O_2-poor atmosphere in comparison to fixed bed reactor experiments (section 3.2), and this promotes an incomplete oxidation of soot producing more CO.

$$nLAMO_3 + C_{soot} \rightarrow nLAMO_{3-2/n} + CO_2 \quad \text{(Step 1)}$$

On the other hand, $C^{18}O^{16}O$ presented a delay with respect to the $C^{16}O_x$ products, indicating that after the cat-soot interaction, oxygen sites became available to be filled in by $^{18}O_2$ from the gas phase. Then, after the $^{18}O_2$ adsorption, and subsequent ^{18}O-^{18}O bond dissociation and exchange with a lattice oxygen, the $^{18}O^{16}O$ molecule is released to oxidize soot particles producing the $C^{18}O^{16}O$ specie. These pathways are summarized in steps 2 and 3. As there is no evidence of $C^{18}O_2$, we concluded that $^{18}O_2$ did not react directly with soot at 400 °C, and the only mechanism at this temperature is the catalytic one.

$$nLAMO_{3-2/n} + {}^{18}O_2 \rightarrow [(n-1)\ LAMO_3]\text{-}LAMO^{18}O_2 \quad \text{(Step 2)}$$

$$[(n-1)\ LAMO_3]\text{-}LAMO^{18}O_2 + C_{soot} \rightarrow [(n-1)\ LAMO_3]\text{-}LAM^{18}O + C^{18}O^{16}O \quad \text{(Step 3)}$$

Guilhaume et al. [6] found similar results for $AgMnO_3$-catalyzed diesel soot combustion with $^{18}O_2$. The authors stated that soot ignition started by the transfer of lattice oxygen to the soot, and once it was transferred, lattice oxygen was rapidly replenished by $^{18}O_2$ from the gas phase, a fact that was evidenced by the simultaneous $^{18}O_2$ consumption and CO_2 formation. By comparing Fig. 7 A and B ($^{18}O_2$ pulsed over LAM-soot and LAM-soot-NO samples respectively), the effect of NO presence during soot oxidation process over LAM catalyst was very important. In this sense, in Fig. 7 B the CO_2 profile presents an additional small and wide peak to the one evidenced in soot oxidation by oxygen (Fig. 7 A). Considering NO presence, the experiment allowed us to conclude that the second CO_2 peak depletion around 40 s (m/z = 44 and m/z = 46), coincided with the end of NO adsorption (m/z = 30 signal) and the maximum of NO_2 released, as Fig. 7 E confirmed, suggesting that soot oxidation in this second stage was promoted by NO_2. This result agrees with the one obtained in the catalytic experiments (Fig. 4) where it was concluded that soot oxidation can be assisted by both active oxygen species (O^-;O_2^-) and NO_2. The reaction pathways for NO_2 release and soot oxidation by NO_2 over LAM catalyst are described in steps 4 and 5. More details about the different NO-adsorbed species on LAM and LM catalyst sites are presented below.

$$nLAMO_3 + NO \rightarrow nLAMO_{3-1/n} + NO_2 \quad \text{(Step 4)}$$

$$2NO_2 + C \rightarrow CO_2 + 2NO \quad \text{(Step 5)}$$

$$NO_2 + 2C \rightarrow 2CO + 1/2N_2 \quad \text{(Step 6)}$$

Reduction of NO_2 to NO, as step 5 indicates, was evidenced in fixed bed reactor experiments where NO was the main nitrogen-gas-specie at reactor outlet. However, $N^{18}O$ presence could not be established by mass spectrometry, due to overlapping of the mass spectra signals. According to the balance of nitrogen-species (see equation S3), there is NO_2 reduction to N_2, for this reason step 6 was considered. N_2 formation was evidenced by gas chromatography as can be seen in Fig. S10.

The results in Fig. 7 B also indicated that the maximum of CO_2 evolution due to soot oxidation by NO_2 had a delay compared to the peak of CO_2 coming from soot oxidation by oxygen species. This result, in addition to the fact that NO adsorption occurred after surface oxygen desorption, as it can be seen in Fig.7B: where NO consumption took longer than oxygen exchange process, about 20 seconds more. Additionally, from figure 7E, NO_2 desorption rate was slower than both oxygen adsorption and release rate, with a NO_2 desorption delay of 30 seconds compared to $^{18}O_2$ profile, which was use as reference. Based on these results, it is concluded that the limiting steps in the soot

oxidation process are the NO adsorption and the following NO_2 release, as has been demonstrated in other studies [44–46]. Similarly, Shen et al. [47] showed that the rate limiting step of NO oxidation over $La_{0.8}Sr_{0.2}MnO_3$ was the desorption of NO_2 from catalyst surface with activation energy of 101.0 kJ mol^{-1}; while activation energy of NO_2 desorption over Pt catalyst ranged from 59 to 81.2 kJ mol^{-1}. Additionally, Wang et al [48] found that NO_2 desorption from manganese nitrates had an energy barrier of 86.8 kJ mol^{-1}; compared with NO adsorption and transformation to nitrates with an energy barrier of 69.5 kJ mol^{-1}, or with O_2 decomposition into atomic O that had an energy barrier of 80.0 kJ mol^{-1}.

Regarding LM-soot-NO test (Fig. 7 D), it is observed that CO_x species evolution has its main peak around 10 s accompanied with a small second peak appearing around 20 s, i.e., that this last peak has a delay with respect to the peak of $^{18}O_2$ profile (use as reference). As this second peak did not appear in the CO_x profiles of LM-soot test (Fig. 7 C), this second CO_2 production was attributed to soot oxidation assisted by NO_2. According with the above results, soot oxidation assisted by NO_2 was more important for the silver containing catalyst (LAM), probably due to a higher NO to NO_2 oxidation capacity. To probe this hypothesis, we performed pulses of $^{18}O_2$ over LAM and LM catalysts, without soot and in presence of NO at 400 °C, Fig. 7 E and F respectively. In these figures, the decrease in the NO signals followed by the evolution of NO_2 indicates that both catalysts oxidize NO to NO_2. Although it was observed that the NO adsorption process over LAM catalyst took about the double of the time than the one required for LM catalyst, the LAM-NO_2 desorption was faster. This characteristic suggest that silver particles play a role in the NO adsorption, and the consequent oxidation to NO_2. To clarify the silver-effect, a DRIFT analysis was performed over both catalysts (Fig. 8). Previous to DRIFT experiments, the sample was pretreated at 500 °C in Ar flow to remove surface-adsorbed species including carbonates. Although it is hard to remove all carbonates during pretreatment, it was found that these surface-remaining species did not interfere in the interpretation of catalytic results, especially during the CO_2 evolution and the subsequent carbonates species formation due to CO_2 re-adsorption coming from soot oxidation. (see Fig. S5).

According to the DRIFT results, NO species formed on LAM catalyst correspond mainly to bridging nitrate (1620 cm^{-1}), chelating nitrates (1587 cm^{-1}) and Ag nitrites species (1390 cm^{-1}), which have less thermal stability than nitrates formed over LM catalyst: free ionic nitrates (1350 and 1390 cm^{-1}) and monodentate nitrate species (1530-1500 cm^{-1}) [48–51]. Even though the overlap of Ag nitrites (1390 cm^{-1}) and free ionic nitrates (1350, 1390 cm^{-1}) species is within the same wavenumber range, the occurrence of each specie depends on temperature, allowing their differentiation. Thus, nitrite species decomposition occurs at low temperatures under soot presence. Once nitrite species are

consumed, the formation of nitrate species on catalyst, which are thermally-stable, are favored over 500 °C [51], see Figure S6 A and B. These results explain the faster NO_2 release (Fig. 7 E) over the silver containing catalyst (LAM). In addition, by plotting the DRIFT signals of nitrogen species (bridging and chelating nitrates and silver nitrites) observed over LAM with temperature (Fig. 8 A and B), it was possible to see the consumption of bridging nitrate (1620 cm^{-1}) and Ag nitrites species (1390 cm^{-1}) between 100 °C and 400 °C [52]. This is consistent with the NO_2 release observed in this range of temperatures (Fig. 4B), and the CO_2 evolution matches with the DRIFT signal observed at 2360 cm^{-1}. On the contrary, nitrogen species adsorbed on the LM catalyst, such as free ionic nitrates (1350 and 1390 cm^{-1}) and monodentate nitrate species (1530 cm^{-1}) [53,54], reached a maximum around 420 °C where NO_2 is released, indicating that NO adsorption and oxidation over LM needs higher temperatures than the process over LAM catalyst. Detailed information of the adsorbed-nitrogen-species and the effect of silver presence on LAM catalyst is widely discussed and presented in our last work [40].

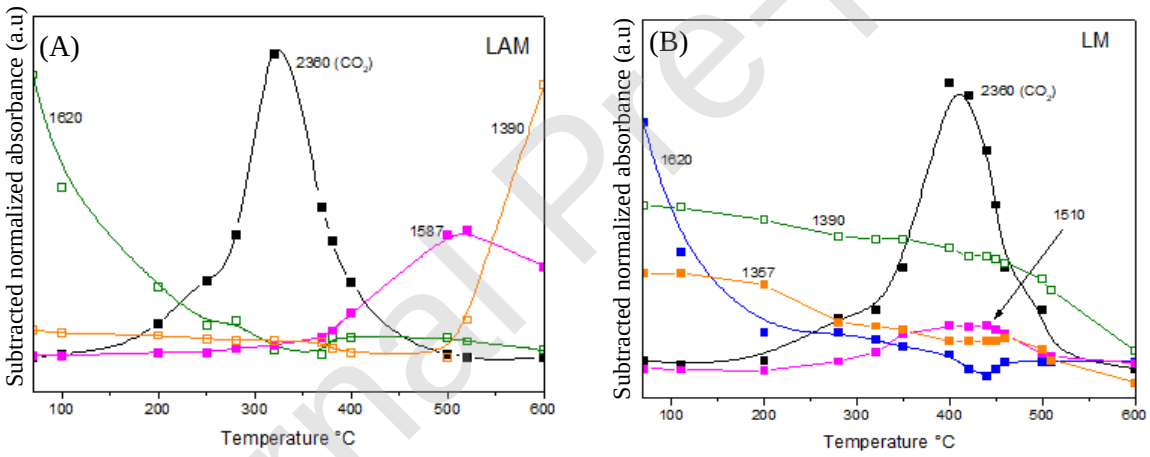

Fig. 8. DRIFT signal profiles with temperature at 1390, 1587, 1620 and 2360, cm^{-1} for LAM catalyst (A); and (B) 1357, 1390, 1510, 1620 and 2360 cm^{-1} for LM sample.

On the basis of DRIFT results, silver in LAM catalyst plays an important role in NO to NO_2 oxidation capacity, influencing its performance to soot oxidation because NO_2 is an important specie to assist this process.

Thus, to have a better insight into catalysts performance due to NO presence, soot combustion experiments were performed in the fixed-bed reactor with inlet NO concentration varied between 0 and 2000 ppm. Fig. 9 (A) summarizes inlet NO concentration effect on soot oxidation by presenting

the temperature of 50 % of soot conversion (T_{50}) against inlet NO concentration. From Fig. 9 A, it is possible to see a decrease in the T_{50} values as inlet NO concentration increases in both catalysts. This is because the higher the NO concentration, the higher the NO_2 production, assisting the soot oxidation process. However, at low inlet NO concentrations the difference in T_{50} between both catalysts was higher (Fig. 9 B). This is because soot oxidation process was more efficient over LAM catalyst due to the higher content of active sites that allowed it to oxidize NO to NO_2 more efficiently. Particularly, when NO inlet concentration was 500 ppm, LAM catalyst has the best catalytic performance, suggesting that over this NO inlet concentration the competence between NO and O_2 for catalyst active sites is higher, making NO_2 evolution less efficient. In fact, according with the results obtained in catalytic experiments, NO to NO_2 oxidation capacity decreases when inlet NO concentration is 2000 ppm. These results highlight the importance of LAM catalysts in the new generation of diesel engines with low NOx emissions.

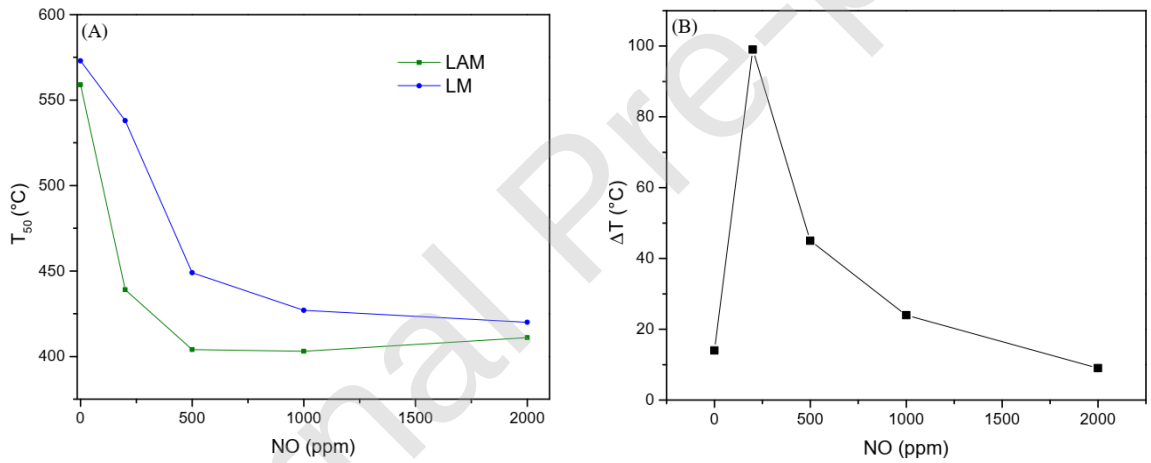

Fig. 9. (A) inlet NO concentration effect over the temperature at which 50 % of the initial soot is converted (T_{50}) over LAM and LM catalyst. (B) difference in T_{50} between LAM and LM catalyst with inlet NO concentration.

3.4 Discussion

According to the isotopic-labelling experiments, the presence of silver into LAM catalyst enhanced the oxygen exchange capacity compared with LM catalyst (see Fig. 6), due to a high increase in active sites formation such as oxygen vacancies, reducible sites (Mn^{4+}) and metallic silver segregated on

catalytic surface (see Table 1). Similar results have been reported by Kucharczyk et al. [55] who made a partial substitution of La^{3+} with Ag^{+} in the $LaMnO_3$ perovskite for improving the oxidation of CH_4. They found that the CH_4 oxidation was shifted to lower temperature when Mn^{4+}/Mn^{3+} ratio was around 1.5 for silver contents into the perovskite lower than 0.3. Yoon et al. [28] also observed that the partial substitution of La^{3+} with Ag^{+} in the perovskite catalyst produced oxygen vacancies as active reaction sites for the NO oxidation with the concomitant transformation of Mn^{3+} to Mn^{4+}. In fact, it was found that the maximum solubility of Ag into the crystal structure of $LaMnO_3$ was achieved at around x = 0.2, where the highest amount of oxygen vacancies was formed.

For catalytic systems different to perovskites, it has been reported that the incorporation of silver into CeO_2 catalyst (CeO_2-Ag) or its segregation on catalyst surface (Ag/CeO_2) improves the oxygen exchange capacity through the formation of active sites for gaseous oxygen adsorption/dissociation resulting in the promotion of superoxide ions (O_2^-) species. According with Yamazaki et al. [56] the active oxygen species formed on the Ag surface migrate to the CeO_2 surface via the interface forming O_2- species, which are then transferred to soot particles where oxidation occurs. Yamakazi et al. [57] found that the spin densities of the O_2^- species formed on the CeO_2-Ag, Ag/CeO_2 and CeO_2 catalyst were 0.83, 0.47 and 0.002 μmol/g, respectively. This trend was the same followed by the catalytic activity, and agrees with the fact that isotopic exchange reaction proceeded fastest over CeO_2-Ag catalyst.

The DRIFT results also indicate that the enhancement in oxygen exchange capacity due to silver presence in LAM perovskite improves the oxidation of adsorbed-NOx species, leading to the formation of chelating and bridging bidentate nitrates, as well as, Ag-nitrites or hyponitrites. These species facilitate NO_2 release at low temperature (< 400 °C). These results agreed with catalytic test results, where the silver containing catalyst (LAM) oxidize NO to NO_2 at lower temperatures and had a better catalytic performance for soot oxidation. Similar results were found by Atribak et al. [18], that studied the catalytic activity for NO_2 production, and the surface processes occurring upon $NO+O_2$ interaction with CeO_2, ZrO_2 and $Ce_xZr_{1-x}O_2$ catalysts. This study found that oxidation of NO to NO_2 follows the same trend of nitrates production and it was affected by the adsorption strength of those nitrates. Hence, Ce-rich catalysts, in comparison with Zr-rich solids, formed ad-NOx species in chelated and bridged configurations. As these adsorbed-species have weak thermostability, Ce-rich catalysts required lower temperatures to transform nitrites into nitrates, explaining their better catalytic activity for NO_2 production.

Fig. 10 shows the reaction pathway proposed in this study based on DRIFTS and isotopic results. In this reaction scheme, we considered all the identified active species for soot and NOx oxidation

formed over the catalyst active sites. First, cat-soot interaction must exist where catalyst oxidizes soot with its ^{16}O-oxygens coming from perovskite, producing $C^{16}O_2$. At the same time, these 16-oxygens also oxidize silver metallic particles segregated on surface catalyst. Then, the oxygen sites generated in these processes become available and are occupied by $^{18}O_2$ coming from gas phase. $^{18}O_2$-adsorbed dissociates on the catalyst and is exchanged with oxygen on the catalyst; then the activated oxygen species are transferred to soot particles producing $C^{18}O^{16}O$.

Meanwhile, in an adsorption/oxidation/desorption process, NO is adsorbed on catalyst active sites already occupied by oxygen either from gas or from perovskite, and on segregated metallic silver forming thermally unstable complexes like bidentate bridging and chelating nitrates, and Ag-nitrites or hyponitrites, which subsequently release NO_2 that assists soot oxidation. Both, oxygen or nitrogen active species released from catalyst surface attack soot sites by forming carbon oxygenated and organic nitro/nitrite complexes that finally produce CO_2 and NO/N_2. After a certain temperature (above 400 °C) nitrogen oxide complexes become ad-species with higher thermostability, such as monodentate nitrates, free ionic nitrates and silver nitrates, that allow catalyst to store NO_x.

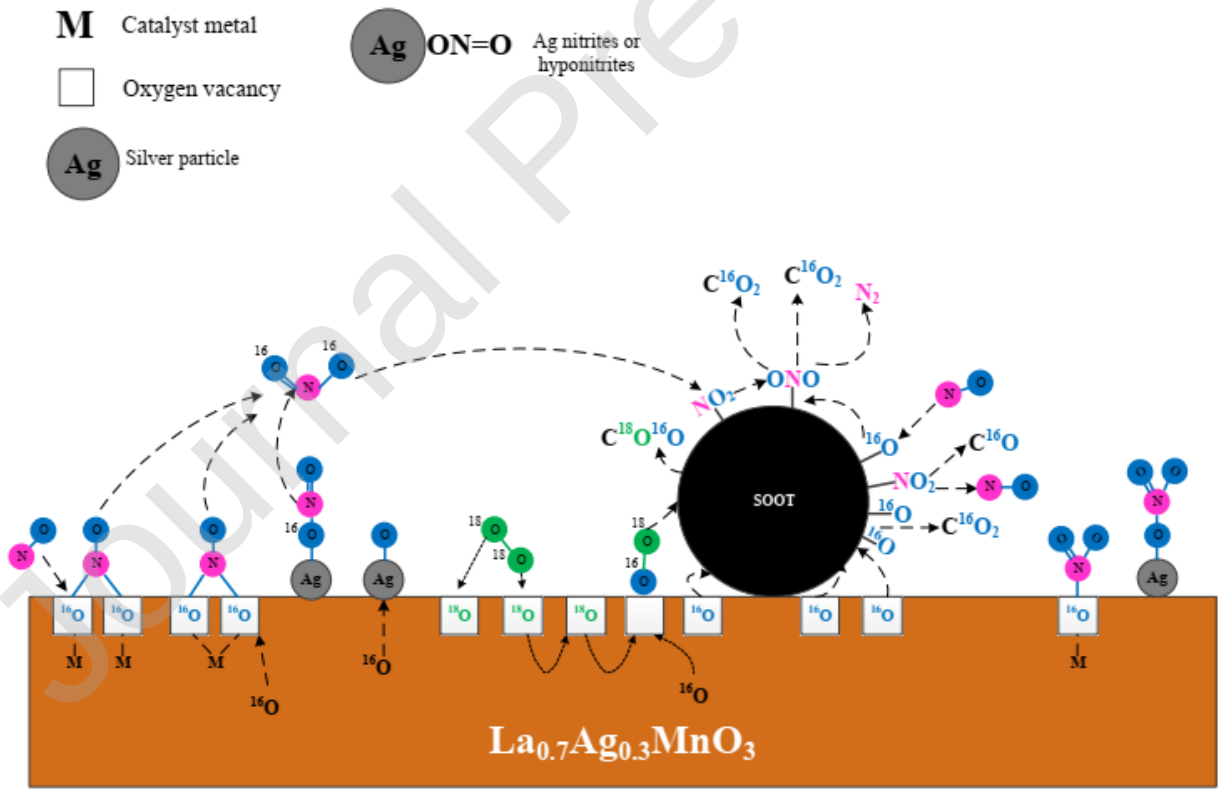

Fig. 10. $La_{0.7}Ag_{0.3}MnO_3$-soot proposed reaction pathway under NO/O_2 atmosphere

4. Conclusions

Soot oxidation with O_2/NO_x has been catalyzed by bare and Ag-doped $LaMnO_3$ perovskites, and the reaction mechanism has been studied paying special attention to the role of oxygen exchange between gas phase O_2 and the catalysts and to the nature of the surface NO_x species present on the catalyst surface under reaction conditions. Main conclusions can be summarized as follows:

Silver loading to the $LaMnO_3$ perovskite allowed the formation of oxygen active sites that enhances the oxygen exchange process between perovskite oxygen and gas phase O_2. According to XPS analysis, these active sites correspond mainly to oxygen vacancies, Mn^{4+}, and metallic silver (Ag^0) segregated on catalyst surface. This improved Ag-promoted oxygen exchange enhances the soot oxidation capacity with regard to the bare $LaMnO_3$ perovskite.

The elucidated reaction-pathway indicated that catalyst oxygen is transferred to soot, and then gas-phase-oxygen occupies the vacancies created. Furthermore, 16-oxygen species coming from catalyst play an important role in the formation of adsorbed NO_x species that lead to NO_2 formation, which also assists soot oxidation.

The desorption of NO_2 is favored by the presence of silver, which promotes the formation of less thermally stable nitrite/nitrates species on oxygen sites and metallic silver in a temperature range from 300°C to 400 °C, which is relevant for soot oxidation process.

CRediT author statement

Laura Urán: Conceptualization, Validation, Formal analysis, investigation, Writing - Original Draft, Visualization, Data Curation. **Jaime Gallego:** Formal analysis, Funding acquisition. **Esther Bailón-García:** Writing - Review & Editing, Validation, Formal analysis **Agustín Bueno-López:** Conceptualization, Resources, Methodology, Validation, Writing - Review & Editing, Funding acquisition. **Alexander Santamaría:** Supervision, Project administration, Funding acquisition

Declaration of interest

none

Acknowledgement

The authors want to thank the University of Antioquia for the financial support received through the CODI project No 2015-7828. L.U. thanks the Colombian Administrative Department of Science, Technology and Innovation (COLCIENCIAS), for the Ph.D. Scholarship granted; to the ENLAZA-MUNDOS program from Mayor's office in Medellín, for the partial-support to an international internship; and to Professor Agustín Bueno from MCMA research group at materials institute of University of Alicante (IUMA), for the international internship.

References

[1] İ.A. Reşitoğlu, K. Altinişik, Keskin.A, Clean Technol. Environ. Policy 17 (2015) 15–27.

[2] F.J. Kelly, J.C. Fussell, Environ. Geochem. Health 31 (2015) 631–649.

[3] N.M. Liu, J. Grigg, BMJ Paediatr. Open 2 (2018).

[4] R. Prasad, V.R. Bella, Bull. Chem. React. Eng. Catal. 5 (2011) 69–86.

[5] B.A.A.L. van Setten, M. Makkee, J.A. Moulijn, Catal. Rev. Sci. Eng. 43 (2001) 489–564.

[6] N. Guilhaume, B. Bassou, G. Bergeret, D. Bianchi, F. Bosselet, B. Jouguet, C. Mirodatos, Appl. Catal. B Environ. 119–120 (2012) 287–296.

[7] G.C. Koltsakis, A.M. Stamatelos, Prog. Energy Combust. Sci. 23 (1997) 1–39.

[8] S. Kumar Megarajan, S. Rayalu, Y. Teraoka, N. Labhsetwar, J. Mol. Catal. A Chem. 385 (2014) 112–118.

[9] P.C. Shukla, in: A.K. Agarwal, J.G. Gupta, N. Sharma, A.P. Singh (Eds.), Springer Singapore, Singapore, 2019, pp. 127–142.

[10] K. Yamamoto, T. Sakai, Catal. Today 242 (2015) 357–362.

[11] K. Krishna, M. Makkee, Catal. Today 114 (2006) 48–56.

[12] M. Piumetti, S. Bensaid, D. Fino, N. Russo, Catal. Struct. React. 1 (2015) 155–173.

[13] G.. Dhal, S. Dey, D. Mohan, R. Prasad, Bull. Chem. React. Eng. Catal. 13 (2018) 144–154.

[14] N. Guillén-Hurtado, A. García-García, A. Bueno-López, J. Catal. Ca 299 (2013) 181–187.

[15] C. Davies, K. Thompson, A. Cooper, S. Golunski, S.H. Taylor, M.B. Macias, A. Tsolakis, Appl. Catal. B Environ. 239 (2018) 10–15.

[16] Z. Wang, X. Yan, X. Bi, L. Wang, Z. Zhang, Z. Jiang, Q. Wang, Mater. Res. Bull. 51 (2014) 119–127.

[17] L. Lietti, L. Castoldi, R. Soc. Chem. 33 (2018).

[18] I. Atribak, B. Azambre, A.B. Lo, Appl. Catal. B Environ. 92 (2009) 126–137.

[19] J. Schobing, V. Tschamber, J.F. Brilhac, A. Auclaire, Y. Hohl, Comptes Rendus Chim. 21 (2018) 221–231.

[20] F. Bin, G.L. Song, J. Song, K. Wang, X. Li, Proc. Combust. Inst. 34 (2013) 2303–2311.

[21] W.F. Shangguan, Y. Teraoka, S. Kagawa, Appl. Catal. B Environ. 12 (1997) 237–247.

[22] A. Serve, A. Boreave, B. Cartoixa, K. Pajot, P. Vernoux, Appl. Catal. B Environ. 242 (2019) 140–149.

[23] M. Zawadzki, W. Staszak, F.E. López-Suárez, M.J. Illán-Gómez, A. Bueno-López, Appl. Catal. A Gen. 371 (2009) 92–98.

[24] S. Royer, D. Duprez, F. Can, X. Courtois, C. Batiot-Dupeyrat, S. Laassiri, H. Alamdari, Chem. Rev. 114 (2014) 10292–10368.

[25] A. Mishra, R. Prasad, Catal. Rev. 56 (2014) 57–81.

[26] K. Wang, L. Qian, L. Zhang, H. Liu, Z. Yan, Catal. Today 158 (2010) 423–426.

[27] L. Urán, J. Gallego, W. Li, A. Santamaría, Appl. Catal. A Gen. 569 (2019) 157–169.

[28] D. Yoon, E. Lim, Y.J. Kim, J.H. Kim, T. Ryu, S. Lee, B.K. Cho, S. Yoo, J. Catal. 319 (2014) 182–193.

[29] W.Y. Hernández, D. Lopez-Gonzalez, S. Ntais, C. Zhao, A. Boréave, P. Vernoux, Appl. Catal. B Environ. 226 (2018) 202–212.

[30] M. Iliev, M. Abrashev, V. Popov, V. G. Hadjiev, Role of Jahn-Teller Disorder in Raman Scattering of Mixed-Valance Magnites, 2003.

[31] J.A. Onrubia, B. Pereda-Ayo, U. De-La-Torre, J.R. González-Velasco, Appl. Catal. B Environ. 213 (2017) 198–210.

[32] T. Andana, M. Piumetti, S. Bensaid, L. Veyre, C. Thieuleux, N. Russo, R. Pirone, Appl. Catal. B Environ. 216 (2017) 41–58.

[33] S. Ponce, M.A. Pena, J.L.G. Fierro, Appl. Catal. B Environ. 24 (2000) 193–205.

[34] J. Chen, M. Shen, X. Wang, G. Qi, J. Wang, W. Li, Appl. Catal. B Environ. 134–135 (2013) 251–257.

[35] B. Kucharczyk, W. Tylus, Appl. Catal. A Gen. 335 (2008) 28–36.

[36] S. Royer, F. Bérubé, S. Kaliaguine, Appl. Catal. A Gen. 282 (2005) 273–284.

[37] P. Xiao, L. Zhong, J. Zhu, J. Hong, J. Li, H. Li, Y. Zhu, Catal. Today 258 (2015) 660–667.

[38] N. Gunasekaran, S. Saddawi, J.J. Carberry, 111 (1996) 107–111.

[39] J. Giménez-Mañogil, A. García-García, Fuel Process. Technol. 129 (2015) 227–235.

[40] D. Martin, D. Duprez, J. Phys. Chem. 100 (1996) 9429–9438.

[41] D. Fino, N. Russo, G. Saracco, V. Specchia, J. Catal. 217 (2003) 367–375.

[42] H.J.M. Bouwmeester, C. Song, J. Zhu, J. Yi, M. Van Sint Annaland, B.A. Boukamp, Phys. Chem. Chem. Phys. 11 (2009) 9640–9643.

[43] A. Bueno-López, K. Krishna, M. Makkee, J.A. Moulijn, J. Catal. 230 (2005) 237–248.

[44] H. Huang, J. Liu, P. Sun, S. Ye, RSC Adv. 6 (2016) 102028–102034.

[45] D. Fino, P. Fino, G. Saracco, V. Specchia, Appl. Catal. B Environ. 43 (2003) 243–259.

[46] Y. Wang, R. Oord, D. van den Berg, B.M. Weckhuysen, M. Makkee, ChemCatChem 9 (2017) 2935–2938.

[47] B. Shen, X. Lin, Y. Zhao, Chem. Eng. J. 222 (2013) 9–15.

[48] W. Wang, G. Yuan, B. Shan, M. Nguyen, U.M. Graham, B.H. Davis, G. Jacobs, K. Cho, Science (80-.). 337 (2012) 832–836.

[49] X. Zhang, H. He, H. Gao, Y. Yu, Spectrochim. Acta Part A Mol. Biomol. Spectrosc. 71 (2008) 1446–1451.

[50] Y. Wen, C. Zhang, H. He, Y. Yu, Y. Teraoka, Catal. Today 126 (2007) 400–405.

[51] L. Urán, J. Gallego, W. Ruiz, E. Bailón-García, A. Bueno-López, A. Santamaría, Appl.

Catal. A Gen. 588 (2019) 117280.

[52] M. Kantcheva, J. Catal. 494 (2001) 479–494.

[53] A. Bueno-lópez, D. Lozano-castelló, J.A. Anderson, Appl. Catal. B Environ. 198 (2016) 189–199.

[54] K. Hadjiivanov, in: Catal. Rev., Taylor, Publisher, 2000, pp. 71–144.

[55] B. Kucharczyk, W. Tylus, Appl. Catal. A Gen. 335 (2008) 28–36.

[56] K. Yamazaki, Y. Sakakibara, F. Dong, H. Shinjoh, Appl. Catal. A Gen. 476 (2014) 113–120.

[57] K. Yamazaki, T. Kayama, F. Dong, H. Shinjoh, J. Catal. 282 (2011) 289–298.

Table 1. Results of the samples characterization by XPS and Raman spectroscopy and specific surface area.

Sample	Ag/Mn[a]	Ag_{perov}	Ag^0/Ag_s[b]	Mn^{3+}/Mn_{tot}	Mn^{4+}/Mn_{tot}	Mn^{4+}/Mn^{3+}	IAg/IB_1g[c]	O_β	O_α	SSA[d]
LM	0.00	0.00	0.00	0.41	0.35	0.85	1.92	0.55	0.24	22
LAM	0.56	0.81	0.19	0.31	0.40	1.28	1.81	0.62	0.33	34

[a] Nominal stoichiometric ratios for $LaMnO_3$ (La/Mn = 1) and $LaAgMnO_3$ (La/Mn = 0.7 and Ag/Mn = 0.3)

[b] Ag_s is the total silver non-incorporated into perovskite-like lattice, i.e. Ag_2O+Ag^0.

[c] Intensity ratio from Raman spectra

[d] Specific surface area obtained from N_2 physisorption using the BET method (m^2/g)

Table 2. CO_x selectivity from LAM and LM-catalyzed soot oxidation experiments in a conventional fixed-bed reactor.

Catalyst	Gas flow	CO_2 selectivity (%)	CO selectivity (%)
$La_{0.7}Ag_{0.3}MnO_3$	10% O_2/N_2	100	0
$LaMnO_3$		100	0
$La_{0.7}Ag_{0.3}MnO_3$	1000 ppm NO/10%	93	7
$LaMnO_3$	O_2/N_2	92	8